Experimental Thermal and Fluid Science 54 (2014) 136–150

Contents lists available at ScienceDirect

Experimental Thermal and Fluid Science

journal homepage: www.elsevier.com/locate/etfs

Experimental study on flow and combustion characteristic of a novel swirling burner based on dual register structure for pulverized coal combustion

Rui Luo, Yafei Zhang, Na Li *, Qulan Zhou, Peng Sun

State Key Laboratory of Multiphase Flow in Power Engineering, Xi'an Jiaotong University, Xi'an 710049, China

ARTICLE INFO

Article history:
Received 23 March 2013
Received in revised form 26 December 2013
Accepted 30 January 2014
Available online 7 February 2014

Keywords:
Swirling burner
Spout structure
Flow
Combustion
Air distribution

ABSTRACT

A novel spout structure which contains dual-gear rings (DGR) and double conical flaring (DCF) for swirling burner is proposed. Flow field outside the novel burner (DGR–DCF burner) is studied in an unconfined environment comparing with a conventional one. The effects of DGR and DCF structures, secondary air distribution and swirling intensity on reverse flow and turbulence are discussed. Results suggest that the novel burner stabilizes reverse flow and enhances turbulence of the flow field under different air distributions and swirling intensities. The novel burner is further studied in a wall-fired pilot furnace. Gas temperature distribution, NO_x emission and unburned carbon in the fly ash are researched. Higher ignition temperature near the burner spout and a more stable temperature field in the furnace is formed with the novel burner. Reduction of NO_x emission and unburned carbon in the fly ash are achieved. The momentum ratio (M) of inner secondary air to outer primary air is defined to uniform the secondary air distribution. Increase of M raises the temperature level near the burner spout. NO_x emission and the unburned carbon in the fly ash both attain their minimum with $M = 4.428$ in the experiment range.

1. Introduction

Coal is the fundamental fossil energy source in the world. The pulverized coal burner is considered as an important combustion equipment which affects the coal combustion efficiency, safe and stable operation of boiler system and pollution emission. Researchers have done a lot of studies on coal combustion and pollution emission control, such as dense-dilute combustion [1], low-NO_x burner [2–6], flow field organization [4–7], flue gas desulfuration [8–11] and denitration [12,13]. Because of its convenient adjustment, lower cost and important effect on combustion, swirling burner of pulverized coal is always a hot topic for thermal engineering researchers. Smart et al. [14] presented the development of a coal fired precessing jet burner, the program of which began in 1994 because of the further incentive for the utility boiler market, and were performed in depth in 1999. They studied the effect of precessing jet momentum ratio and gun position on NO_x emission, heat flux and ignition distance in detail. The results showed a positive influence of the use of precessing jet on combustion characteristic. Costa et al. focused on the gas temperature and species in the burner region of a front wall fired boiler. They obtained temperature level in the burner region and NO_x concentration above the boiler nose in 1997 [15]. The work provided a considerable effort to minimum variations on boiler operating conditions and a reference for 3D mathematical model evaluation and development. Bollettini et al. [16] operated a study on scaling of natural gas burners and integrated substantial experimental data from scaling 400 projects with CFD simulation in 2000. In 2001 Milani and Saponaro introduced the dilute/flameless combustion technology and the high velocity burners, the emphasis of which is on fluid dynamic entrainment and mixing of flue gases. The temperature distribution of flameless combustion was different with conventional flame combustion and the NO_x formation was controlled [17]. Nettleton studied the effect of swirling angels of secondary air stream on flame stability and suggested some explanation for the existence of stability limits in 2004 [18]. Gu et al. analyzed the relation among the NO_x formation, gas flow and pulverized coal moving in a swirling burner with numerical simulation. The authors found that the maximum particle penetration depth into the internal recirculation zone (IRZ) L_{dav} and effective time of IRZ τ_{eav} lead to the minimum outlet NO emission [19]. Chacón et al. developed a new methodology for the design and optimization of a low NO_x-CO, natural gas burner by numerical simulation to comply with NO_x emission limits of European countries [2]. Jing et al. researched the effect rules of outer secondary air

* Corresponding author. Tel.: +86 29 82668174; fax: +86 29 82668703.
E-mail address: lyna@mail.xjtu.edu.cn (N. Li).

http://dx.doi.org/10.1016/j.expthermflusci.2014.01.021
0894-1777/

Nomenclature

DGR	dual-gear rings
DCF	double conical flaring
IPA	inner primary air
OPA	outer primary air
ISA	inner secondary air
OSA	outer secondary air

Symbols

R	dimensionless radial distance outside the burner (–)
r	radial distance outside the burner (m)
X	dimensionless axial distance outside the burner (–)
x	axial distance from the burner (m)
d	diameter (m)
u	axial velocity (m/s)
U	dimensionless axial velocity (m/s)
V	total air flow rates (Nm^3/s)
v	tangential velocity (m/s)
u'	axial velocity turbulence (m^2/s^2)
v'	tangential velocity turbulence (m^2/s^2)
ε	turbulence intensity (–)
ρ	density (kg/m^3)
Q	air quantity (kg/s)
f_{re}	dimensionless section reverse flow ratio (–)
M	momentum ratio of inner secondary air to outer primary air (–)
Ω	combination swirl intensity (–)
A	cross section area of pipe (m^2)
a	depth of furnace (m)
x', y', z'	depth, width and height coordinate of the furnace (m)
X', Y', Z'	dimensionless depth, width and height of the furnace (–)
w	mass fraction (%)

Subscripts

1,2,3,4	IPA, OPA, ISA, OSA
eq	Equivalent
ct	Axis
o	Outer
i	Inner
fh	Fly ash

vane angels and primary air ratio on flow, combustion characteristic and NO_x emission [6,20]. Li et al. studied the furnace temperature, heat flux and char burnout with double swirling flow burner at different loads [21].

To improve both the combustion performance and NO_x emission, optimizations of swirling burner structure for pulverized coal are proposed and studied continuously. The Babcock & Wilcox Company in New Orleans, LaRue and Wolf [22] proposed an improved burner with a splash plate, deflector and a diffuser to decrease the nozzle pressure drop and NO_x formation in 1983. Babcock-Hitachi Kabushiki Kaisha in Tokyo [23] provided a coal combustion apparatus for NO_x reduction which comprises coal pipe, multi-air passageways and bluff body in 1985. Stein Industrie in France [24] provided an axial conduit for feeding fuel in 1987, which is adjustable for varying the preliminary mixing chamber length and supports the ignition and combustion. The Babcock & Wilcox Company also in 1989 proposed a flame stabilizing ring and retractable gas element to create a low oxygen/fuel rich flame resulting in reduced NO_x formation [25]. Tenova also started in 2002 a research program, which led to a new family of low NOx burners named FlexyTech® TSX based on the flameless technology which allows to reach a low NO_x emission [26]. Orfanoudakis et al. have studied the effect of swirl number on flow and particle characteristic especially near internal recirculation zone (IRZ) in the near-burner region of a multi-fuel laboratory burner in 2005 [27]. Li et al. in 2008 made a comparison between an enhanced ignition-dual register (EI-DR) burner and centrally fuel rich (CFR) swirling burner experimentally on combustion characteristic, and found that CFR burners have higher combustion efficiency, less NO_x emission and more stable flame at low load in a 300 MW(e) wall-fired utility boiler [3]. To burn low rank coal centrally-fuel rich swirling coal combustion burner was proposed and studied both experimentally and numerically by Chen et al. [5]. They focused on the gas-particle flow analysis to control the gas temperature level and NO_x formation. With development of measurement technology and numerical calculation, the investigations on swirling burners become more comprehensive. Allouis et al. proposed a new diagnostic tool based on fast infrared imaging to test the combustion stability for burners and help adjusting flame [28]. Khanafer et al. used computational fluid dynamics simulation coupled with chemical equilibrium calculation to analyze NO_x formation in swirling burners [29]. All the studies on the swirling burner mentioned above have mainly focused on the effects of air distribution, swirling intensity and retrofit structures on combustion and NO_x emission.

However, little study of novel flame ring and flaring effect on the swirling burner, which have significant impact on flow and combustion, has been reported. In this paper, a novel burner spout with dual-gear rings (DGR) and double conical flaring (DCF) is proposed as shown in Figs. 1 and 2. Cold air test and combustion experiment are carried out under different secondary air distributions, swirling intensities and coal types. The flow characteristic, combustion performance and NO_x emission are discussed. Comparing with a conventional one, the novel burner is proved to be helpful to obtain stable, efficient and clean combustion for pulverized coal.

2. Novel burner model

The proposed novel structures were installed on a radial dual register burner, which is geometric similarity with the ratio of 1:6 to the prototype, the dual register swirling burner of

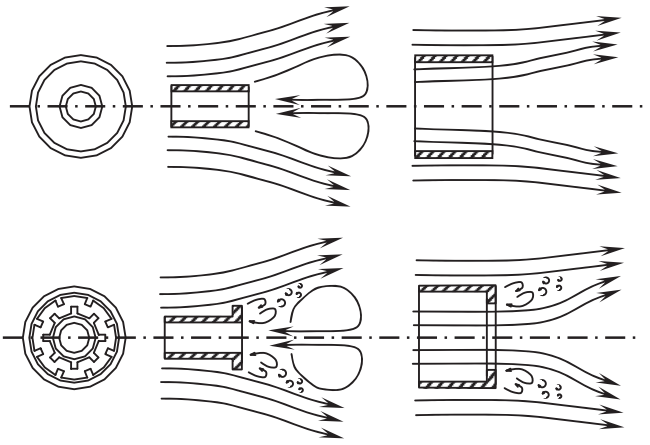

Fig. 1. Design concept of DGR in inner primary air pipe (a) traditional inner primary air spout (up); (b) DGR in the inner primary air spout (down).

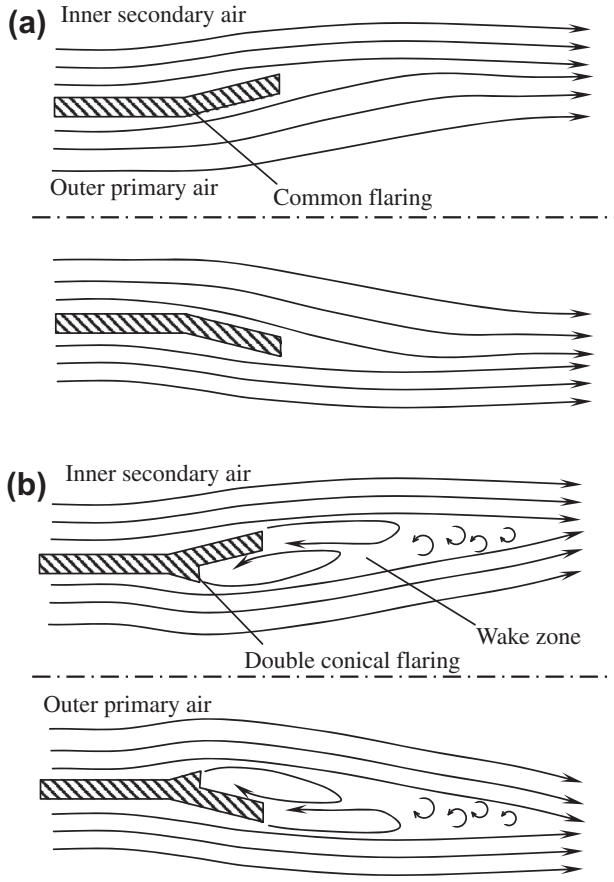

Fig. 2. Design concept of DCF on the outer primary air pipe (a) traditional spout (up); (b) DCF spout (down).

WGZ1246/18.-1 boiler made by Wuhan Boiler Group Co., Ltd. in China. DGR was set in the inner primary air pipe outlet in order to enhance the turbulence and mixing of primary air and pulverized coal in the fuel-rich and oxygen-lean zone in Fig. 1. DCF was set on the outer primary air pipe, so as to induce outer primary air towards center recirculation zone and delay the mixing of secondary air and primary air as Fig. 2 shows. The novel burner spout is expected to reduce the ignition heat and form a fuel-rich field near the spout in the ignition zone.

Fig. 3 shows the schedule drawing of the novel burner model. Inner and outer primary air is separately compelled into the burner with pulverized coal, and reorganized by DGR and DCF at the burner spout. Inner secondary air forms a gust of swirling air flow through the swirling vane and flaring-oriented flow off the burner, so the recirculation zone outside the burner is produced. By moving the swirling vane axial position in the inner secondary air channel, the total swirling intensity can be changed. Outer secondary air flows off the spout as direct-flow to supply oxygen in the later stage.

3. Cold air test study

3.1. Cold air test procedure and methods

Due to the limitation of flow field measurement under a practical combustion state, the isothermal modeling experiment is usually operated to study the flow characteristic [5,30]. According to the modeling principle [31], the air flow with more than 1.0×10^5 of the critical Renolds number to second self-modeling zone was selected.

In this test as shown in Fig. 4, air is compressed by a draft fan and conveyed through tubes to the bellow in which the air was distributed into different ducts as primary and secondary air. Air distribution is controlled by valves, supervised by flow meters and measured by hot wire anemometers.

A dimensionless coordinate is built with R and X in two directions for describing flow field position. $R = r/d_3$, and $X = x/d_3$, where r represents the radial distance off the central axis of the burner, x stands for the axial distance off the end of the burner's jet, while d_3 is the diameter of ISA duct.

Two sets of measuring point arrays were introduced. A 6×31 array was set next to the burner spout in which the radial distance between two closed measuring points was $\Delta R = 0.1$, while the axial distance was $\Delta X = 0.3$. Meanwhile, a 5×29 array was set after in which $\Delta R = 0.2$ and $\Delta X = 1.0$.

A 1050A type dual-channel hot wire anemometer with the range of 0–30 m/s and resolution of 0.01 m/s was used to measure velocity and turbulence instantaneously, while the direction of velocity was obtained by ribbon tracer method. The measurement error is 5% of indication or 0.025 m/s under the temperature range from 18 °C to 93 °C. The turbulent intensity (ε) was calculated with root mean square table supplied by TSI Inc. as Eqs. (1) and (2) shows.

$$u_{eq} = Q/(\rho \pi d_3^2/4) \tag{1}$$

$$\varepsilon = (u' + v')^{0.5}/u_{eq} \tag{2}$$

where u_{eq} is reference velocity. Q is the total air quantity. ρ and d_3 represent the air density and ISA tube diameter, respectively. u' and v' are the axial and tangential velocity turbulence.

The dimensionless axial velocity (U_{ct}) on the axis is defined to analyze the length and position of central recirculation zone as Eq. (3) shows. The dimensionless maximal section velocity (U_{max}) is defined to characterize the attenuation of velocities and mass transfer ability in later period as Eq. (4) shows.

$$U_{ct} = \frac{u_{ct}}{u_{eq}} \tag{3}$$

$$U_{max} = \frac{u_{max}}{u_{eq}} \tag{4}$$

where u_{ct} and u_{max} represent the axial velocity on the axis and maximal axial velocity in one section, respectively. The dimensionless section reverse flow ratio f_{re} is defined in Eq. (5), which illustrates the relative reverse flow quantity in a section.

$$f_{re} = \frac{\sum_{u<0} \rho u \pi (r_o^2 - r_i^2)}{\sum \rho u \pi (r_o^2 - r_i^2)} \tag{5}$$

The section total turbulence intensity ε_{total} can be obtained with weighted summation of the turbulence intensities of all the measurement points in one section, and is expressed as Eq. (6). It represents the fluid macroscopic kinetic dissipation.

$$\varepsilon_{total} = \frac{\sum \varepsilon \pi (r_o^2 - r_i^2)}{\pi d_4^2/4} \tag{6}$$

where u means the axial velocity of flow field. The variables r_o and r_i respectively represent the outer radius and inner radius of the annular area represented by the measure point. d_4 is the outer secondary air pipe diameter. ε_{ct} defined as the turbulence intensity of each section axis represents turbulent and transport ability inside the recirculation region. ε_{max} defined as the maximal turbulence intensity in each section reflects the turbulent and transport ability near secondary air flow.

Because of the air inlet momentum impact on the flame obviously [32], the momentum ratio of inner secondary air to outer

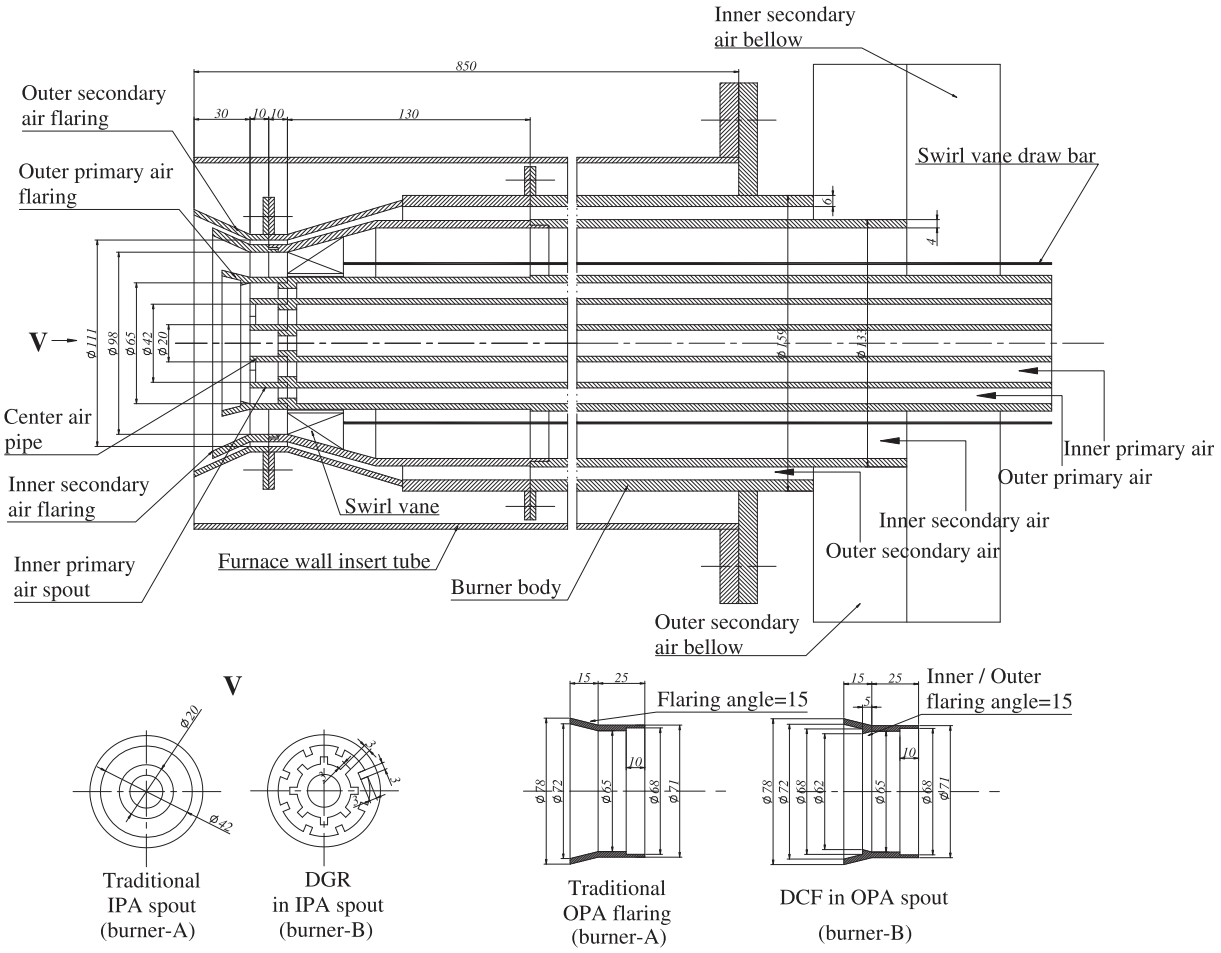

Fig. 3. Cross-section and model size of the A-burner and B-burner.

primary air is expressed as follows, which can be used to uniform the secondary air distribution.

$$M = \frac{\rho_3 u_3^2}{\rho_2 u_2^2} \tag{7}$$

where ρ_2, ρ_3, u_2, u_3 represent the density of outer primary air and inner secondary air, the axial velocity of outer primary air and inner secondary air, respectively.

$$\Omega_c = \frac{\sum_{j=1}^{4} \rho_j u_j v_j A_j r_j}{\sum_{j=1}^{4} \rho_j u_j^2 A_j r_j} \tag{8}$$

Weighted combined swirling intensity Ωc is proposed to describe the swirling level of multilayer coaxial rotary jet from swirling burner, as Eq. (8) shows. The variables of ρ_j, u_j, and v_j represent the density, axial velocity and tangential velocity of the air in a certain layer, respectively. A_j is the cross section area of the air pipe and r_j represents the pipe radius of a certain layer in the swirling burner.

The conventional burner and the novel swirling burner with DGR and DCF are separately called A-burner and B-burner in this paper. The reverse flow and turbulence characteristic were studied and compared between A and B burner under different spout structure, secondary air distribution and swirling intensity conditions, respectively. 12 cases listed in Table 1 were operated in the cold test.

3.2. Aerodynamic characteristic compare

The aerodynamic field is affected by the novel burner spout. Fig. 5 shows the velocity and turbulent intensity distributions for case01 and case04, respectively. The dash lines label the boundary of central recirculation zone outside the two burners. The magnitude of axial and tangential velocity is enlarged by the novel spout. Especially in the central recirculation zone, the reverse flow velocity increases with B-burner spout. The width and length of central recirculation zone induced by B-burner are both smaller than that induced by A-burner. However, B-burner has a comparative width of reverse flow zone near the spout, where $X = 0.3$ shown in Fig. 5(a) and (b). The results of flow field suggest that the reverse flow of B-burner is preferable. Turbulence intensity fields of the two burner spouts are directly compared in Fig. 5(c). The turbulence intensity outside B-burner spout is totally higher than that outside A-burner spout, especially in the reverse flow zone near the spout. The turbulence in the reverse flow zone could improve mixing of the pulverized coal and oxygen which is in favor of combustion. It can be observed that intense turbulence intensity is kept from the cross-section $X = 0$ to $X = 1.5$ for B-burner spout, as is kept from $X = 0$ to $X = 0.9$ for A-burner spout. Therefore, turbulence in later period is believed to be more intense for B-burner spout, which is helpful for fuel to mix with oxygen. It indicates B-burner organizes a more effective flow field for combustion in later period.

A detailed study on novel spout structures is carried on. Four burner spouts are tested for case01–case04. DGR enhances both the reverse flow and turbulence near the spout. The case2 in

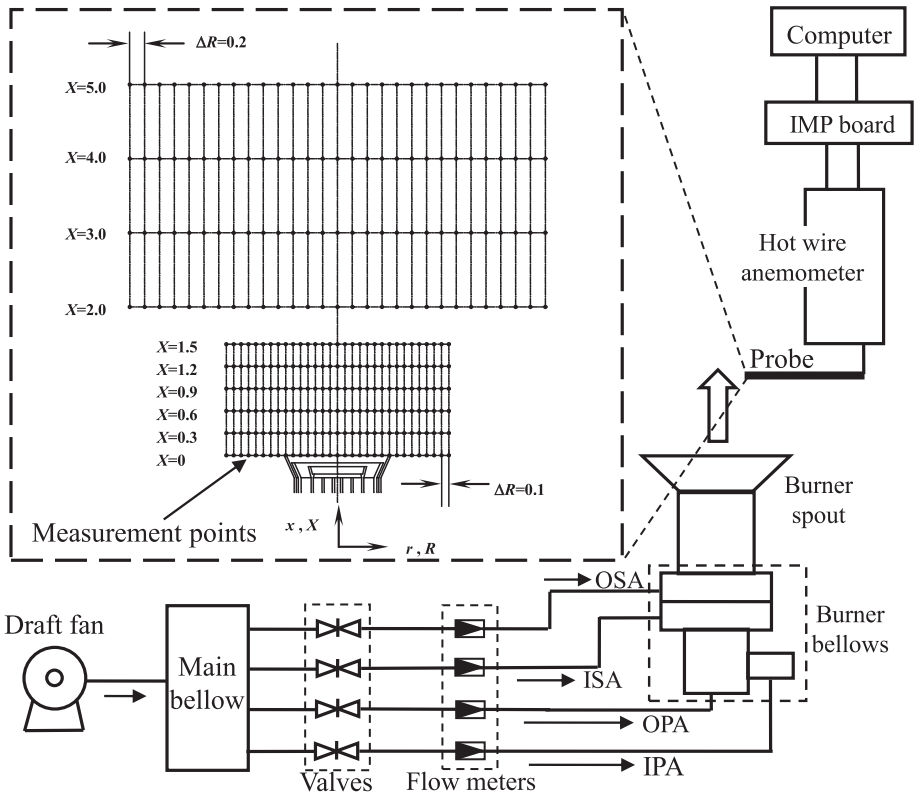

Fig. 4. Cold air experiment system.

Table 1
Operating conditions in aerodynamic experiments (Ω_1, Ω_2, $\Omega_4 = 0$, $V = 0.235$ N m^3/s).

Cases	DGR[a]	DCF[b]	Air ratio				Ω_3	Ω^c	M^d
			Inner primary air (%)	Outer primary air (%)	Inner secondary air (%)	Outer secondary air (%)			
Case01	Disuse	Disuse	10	10	60	20	2.2	1.31	6.378
Case02	In use	Disuse	10	10	60	20	2.2	1.31	6.378
Case03	Disuse	In use	10	10	60	20	2.2	1.31	6.378
Case04	In use	In use	10	10	60	20	2.2	1.31	6.378
Case05	Disuse	Disuse	10	10	70	10	2.2	1.88	8.682
Case06	Disuse	Disuse	10	10	50	30	2.2	0.72	4.428
Case07	In use	In use	10	10	70	10	2.2	1.88	8.682
Case08	In use	In use	10	10	50	30	2.2	0.72	4.428
Case09	In use	In use	10	10	60	20	0.95	0.57	6.378
Case10	In use	In use	10	10	60	20	0.52	0.31	6.378
Case11	Disuse	Disuse	10	10	60	20	0.95	0.57	6.378
Case12	Disuse	Disuse	10	10	60	20	0.52	0.31	6.378

[a] Dual-gear rings.
[b] Double conical flaring.
[c] Weighted combined swirling intensity.
[d] Momentum ratio of inner secondary air to outer primary air.

Fig. 6(a) shows the highest reverse flow velocity on the axis near the spout, which helps inducing hot gas for ignition. This is because inner gear ring of DGR enlarges the diameter of center pipe like the annular bluff body which is in favor of reverse flow. But the length of central recirculation zone just reaches about $X = 2$ outside the burner, shorter than that for any other cases. DGR can enhance the turbulence intensity near the spout, as case02 shows in Fig. 6(b–d). The gear rings decrease the area of inner primary air pipe, which can increase the flow velocity of that layer. Moreover, air flow would produce some vortex through DGR, as Fig. 1 shows. Therefore, the turbulence enhancement near the burner is obtained.

The structure of DCF extends the reverse flow zone. The case03 in Fig. 6(a) shows that axial velocity on the burner axis keeps minus until $X = 5$, which is further than any other cases from spouts. It is believed that DCF can delay the mixing of outer primary air and inner secondary air, and the swirling effect of inner secondary air is kept longer. Meanwhile, DCF enhance the sectional turbulence near and far from the spout. The results of case03 in Fig. 6(b) and (c) imply higher turbulence value than that of case01 near the burner. Fig. 6(b–d) show the highest turbulence level for case03 in the field of $X \geqslant 2$. The double expanding direction of DCF guides outer primary air flowing inwards and inner secondary air flowing outwards, so the mixing of primary air and secondary air delays. It is benefit for keeping jetting rigidity and intense turbulence of the outer secondary air far away from the spout.

Both the sufficient reverse flow velocity and area of the central recirculation zone near the burner are obtained by the novel

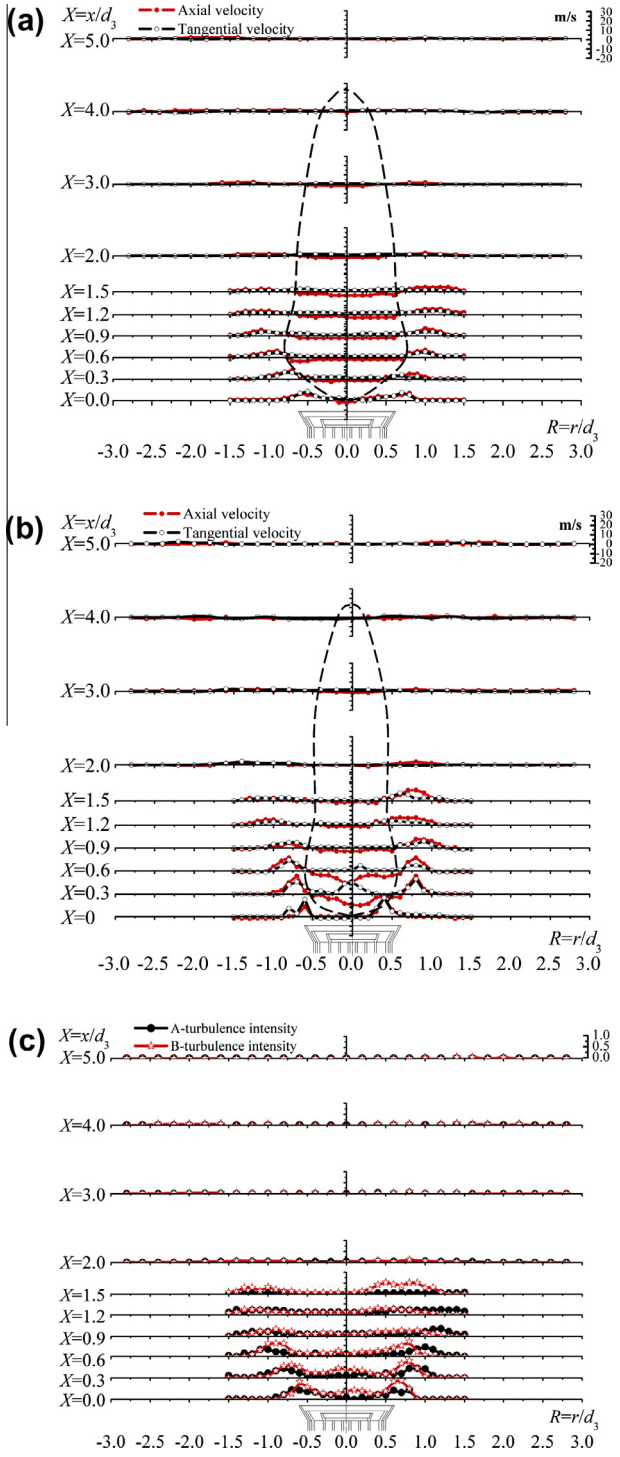

Fig. 5. Velocity and turbulent intensity distributions of the two burners (a) velocity distribution of A-burner; (b) velocity distribution of B-burner; (c) turbulent intensity distribution of A/B- burner.

burner with DGR and DCF. In Fig. 6 the effects of reverse flow for case04 are preferable, and turbulence level is kept favorable near and far from the spout. In conclusion, the novel structure can help to organize a reasonable flow field for ignition and combustion.

Secondary air distribution has little effect on the reverse flow and turbulence characteristic of B-burner. The ratio of inner secondary air to outer primary air M is used to uniform the operating conditions. Fig. 7 shows reverse flow ratio and total turbulence change under different air distribution conditions. The dotted line marks the main reverse flow zone location outside the burner in Fig. 7(a) and (c). Comparing with results in Fig. 7(a), a closer distance of the main reverse flow zone to the burner spout and more reverse flow in Fig. 7(c) indicate B-burner is superior to A-burner. Under different secondary air distributions, the main reverse flow zone are all between $X = 0$ and $X = 1.5$ for B-burner. The turbulence intensities near the spout of B-burner are obviously improved under different air distributions in Fig. 7(b) and (d), which indicates that a stable and favorable turbulence field is organized by B-burner.

Fig. 8 displays the impact of swirling intensity on reverse flow and turbulence of A-burner and B-burner. Fig. 8(a) and (c) shows that increase of swirling intensity raises the reverse flow ratio obviously. B-burner makes the reverse flow zone nearer to the spout and enhances the reverse flow ratio. The total sectional turbulence outside B-burner in Fig. 8(d) is more intense than that outside A-burner in Fig. 8(b) under the three swirling intensity conditions significantly.

Whatever how air supply varies, the sufficient reverse flow and intense turbulence near the spout of B-burner always exist. All mentioned above suggest that B-burner can organize a more efficient reverse flow, stronger turbulence field and more stable flow field under different air distributions and swirling intensities. The further study on the B-burner is conducted in the next section to discuss its organization performance for combustion.

4. Combustion experiment study

4.1. Combustion experiment procedures

This pilot scale furnace is designed according to the similarity and modeling principles [31]. The burner geometric similarity is selected as 1:6. The concentration, density and fineness of coal are similar with that of the actual fuel. The Renold number of air flow exists in the second self-modeling zone. The jetting momentum flow ratio is set similar to the actual conditions. The diffusion time can be also considered similar with actual combustion. However, the residence time may be shorter than that of prototype which could affect the burnout. Moreover, the chemical dynamic similarity and heat transfer similarity are both satisfied in the experiment through controlling the diffusion zone of combustion and selecting appropriate plan heat release rate.

Fig. 9 shows the schematic of the test facility for a 0.7 MW wall fired pilot furnace with the height of 3.2 m. The lower furnace under the throat with a height of 1.75 m and a cross sectional area of 1.00 m × 0.80 m is the fuel-burning zone, which is surrounded by refractory bricks with a thickness of 0.5 m for heat preservation and insulation. Two swirling burners are fixed symmetrically in the center of the front and rear wall separately and the distance between the opposing spout is 1.00 m. The burner axis is 1.00 m height from the first platform. The upper furnace is burnout zone with a height of 1.15 m and a cross sectional area of 0.5 m × 0.80 m above the second platform. It is surrounded by refractory cement with a thickness of 0.25 m for heat preservation. The unburned carbon in the fly ash and pollution emission are measured in this zone. Four spiral micro-quantity feeders on the second platform are used to supply pulverized coal quantitatively. Two different types of pulverized coal are burned separately. The total feeding rates are separately 139.53 kg/h for Tongchuan meagre coal and 87.73 kg/h for Shenmu bitumite coal. The combustion air of 120 ± 5 °C is supplied by air blower for burners with the excess air coefficient of 1.2 after through the air heater. The flue gas is discharged by an induced draft fan through the stack. An axial flow water-pump is adopted to supply cold water to economizers and water jacket of measuring appliances. There are some test hole in

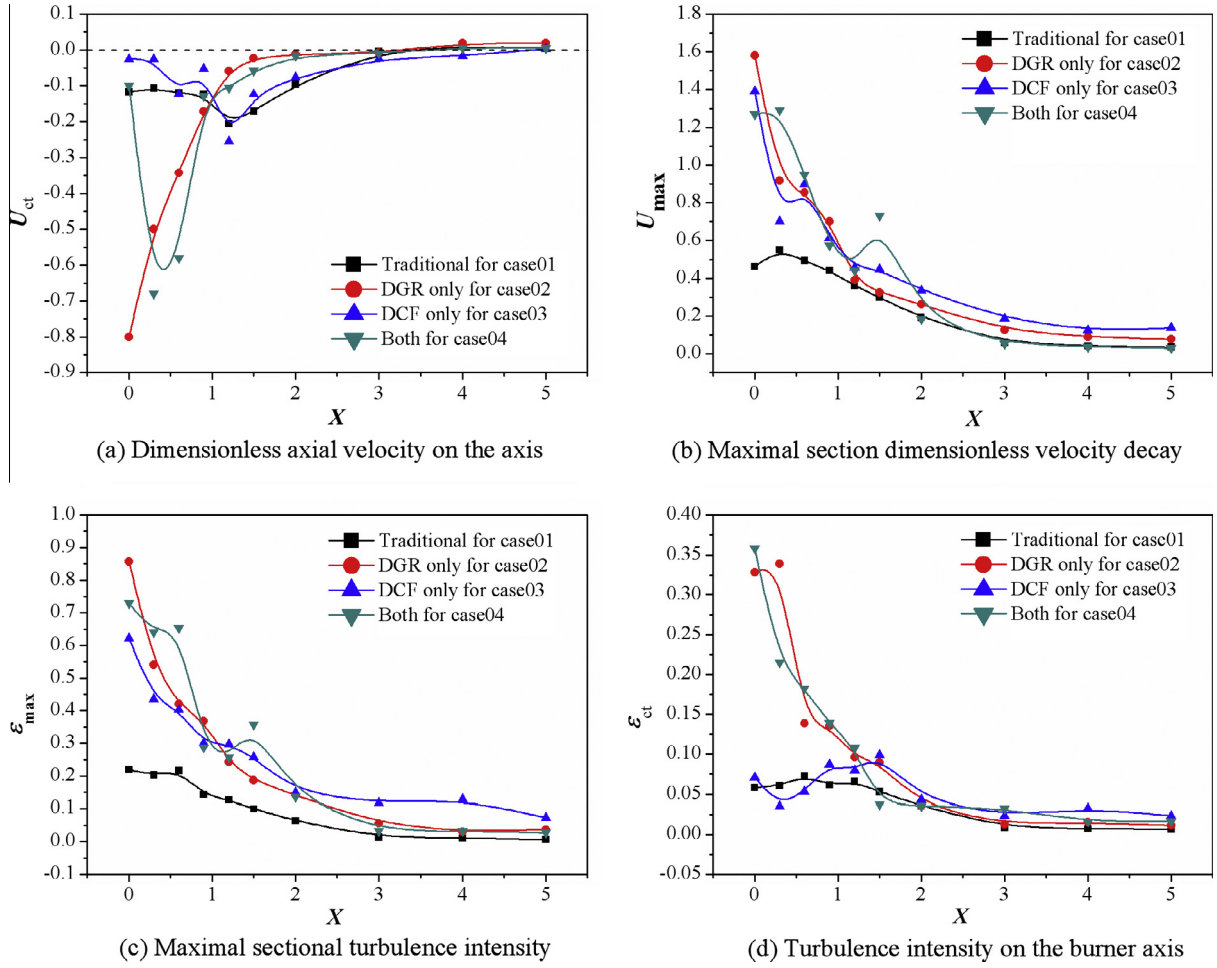

Fig. 6. Effect of different burner structures on aerodynamic characteristic for case01–04.

the furnace wall shown in Fig. 9 for ignition, observation and measurement. Other detailed parameters of operating conditions are shown in Table 3.

The mid-point of the segment on the burner axis in the furnace is selected as the origin of the coordinate shown in Fig. 9(b) and (d). And the dimensionless depth, width and height of the furnace are described as $X' = x'/a$, $Y' = y'/a$, $Z' = z'/a$, where a is the depth of furnace as a reference size.

The flue gas temperature in the lower furnace was measured with the water-cooled standard PtRh10-Pt thermocouple shown in Fig. 10. The whole thermocouple was protected by cooling water and the temperature data was obtained with an accuracy of relative error 1% below in the lower furnace. It was inserted into the furnace chamber from the several test ports arranged on the right wall of the furnace in the experiment. To avoid the effect of measuring stick on ignition and temperature field, only one water-cooled thermocouple was used to measure each point in turn. When it was pulled out of the test hole, the temperature dropped sharply. After it was pushed into another test hole, the temperature increased quickly and reached stable stage after about 20 s. In the combustion experiment, the temperature measurement was required to last 30 s stationary stage so as to obtain efficient data. Therefore, the measurement time in each point is 50 s. Because the measurement stick did not leave the furnace for Y-direction measurement, the response time for temperature measurement here was shorter. The measurement along the furnace width (Y-direction) in the same test hole for obtaining cross-section temperature field had the same measurement time as that along the burner axis. The upper furnace central gas temperature was measured with NiCr–NiSi thermocouples nested in the porcelain sleeves under 1250 °C with an accuracy of relative error 3% below in the upper furnace. All the temperature measurement frequencies were 1 Hz.

The temperature measurement points on the burner axis were located with equal interval of $X' = 0.2$. As Fig. 9(b) shows, the water-cooled thermocouple was inserted into the test hole A∼E in turn for measuring temperature change on the burner axis. The temperature distribution with the furnace height was measured along the centerline of the furnace in Fig. 9(d). The water cooled thermocouple was inserted into the test hole C, F∼H in turn for measuring lower furnace point. We also changed the measurement stick position along the width direction of furnace with an equal interval of $\Delta Y' = 0.07$. The cross-section of $X' = 0$ is divided by 4×11 points and the cross-section of $Z' = 0$ is divided by 5×11 points. The point management and procedure on the cross-sections are detailed in Fig. 9(c) and (e). The five NiCr–NiSi fixed thermocouples were inserted into the test hole 1–5 for measuring temperature change with height in the upper furnace.

The primary air and secondary air rate into the furnace were measured by calibrated back to back pitots, with an accuracy of ±3.5%. The gas and fly ash in the furnace outlet are sampled in the constant-velocity sampling principle using two water-cooled stainless probes in the position of $Z' = 2.30$ on the centerline of furnace, respectively, as Fig. 9(d) shows. The sampling gas composition was measured by MSI-Compact flue gas analyzer with an accuracy of ±0.3 vol% for oxygen and GASMET-DX4000 flue gas

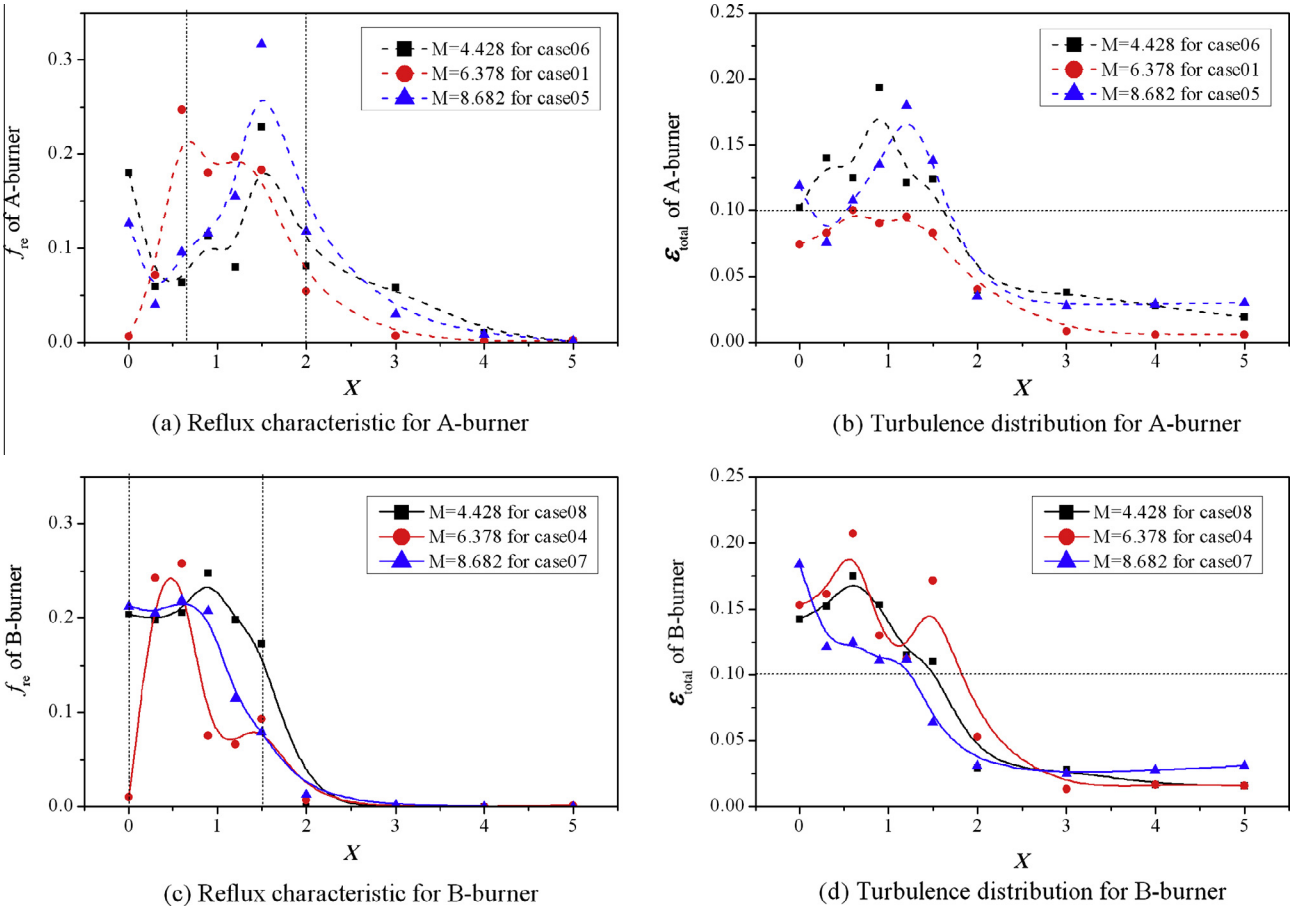

Fig. 7. Effect of air distribution on flow characteristic of A and B burners.

analyzer with an accuracy of ±2 vol% for other species. The unburned carbon was investigated by gravimetric determination method using fly ash sampling. The basic analysis of two coals, Tongchuan (TC) meager coal and Shenmu (SM) bituminous coal used in this experiment are shown in Table 2. The fuel characteristics such as fineness, density and concentration used here are the same as those employed in practice.

In this experiment the flue gas temperature and NO_x emission are mainly measured and compared between the two swirling burners. The effect of secondary air distribution on combustion performance of the novel burner is discussed.

4.2. Combustion characteristic compare

In this section the proposed novel burner (B-burner) is studied in the combustion experiment comparing with the conventional one (A-burner) under the same size as in the cold air experiment. Fig. 11 shows the temperature distribution on the axis of burners. The gas of more than 850 °C is obtained near the spout of B-burner when burning bitumite, while the gas temperature near the spout of A-burner is about less than 800 °C. In the furnace center for $X' = 0$ the B-burner organized a higher flame temperature than A-burner with burning bitumite in Fig. 11(a). When burning meager coal, the gas temperature level on the burner axis becomes lower because of the difficult-flammable coal. If we define the ignition point as above 700 °C, it is obviously observed that the B-burner ignites meager coal earlier than A-burner from Fig. 11(b). B-burner also gets a higher temperature level in the axis center with burning meager coal. Results suggest that ignition for B-burner happens earlier than that for A-burner [33]. Moreover, comparing with burning bitumite, both A and B burner will delay the meager coal ignition because of the low volatiles and heat value per unit mass of meager coal. However, B-burner shows a better performance of burning difficulty-flammable coal than A-burner from the axis temperature compare. The reverse flow velocity and turbulence outside the B-burner spout are proved to be improved in Section 3.2. The mixing of primary air and secondary air delays by DCF and a fuel-rich zone is formed in the center recirculation zone by the novel structure DCF. Pulverized coal can contact oxygen in time under fuel-rich zone and a favorable ignition ring appears near the vortex caused by the novel structure DGR. The coal will be burnt to release heat earlier. Moreover, temperature level on the burner axis with burning bitumite is higher than that with burning meager coal, because the bitumite has more volatile and releases more heat in the early stage of combustion.

The mixing of fuel and air in the middle and later period is enhanced by B-burner. The pulverized coal combustion process along the furnace can be observed in Fig. 12. Because of our experimental facility is much smaller than the large scale one, the temperature level in the furnace is considered more sensitive to the design of burner than that in the large scale facility. The temperature difference level could appears more obvious in this experimental furnace than that in the large facility. Under the same thermal load of the facility, higher temperature level is obtained by B-burner in the furnace on both conditions of burning bitumite and meager coal. It indicates that pulverized coal releases heat adequately after reacting with oxygen outside B-burner. In the lower furnace the temperature level is about 150 K higher with B-burner than that with A-burner for burning each coal. It suggests that B-burner helps mixing of coal volatile and air. It can be observed that in

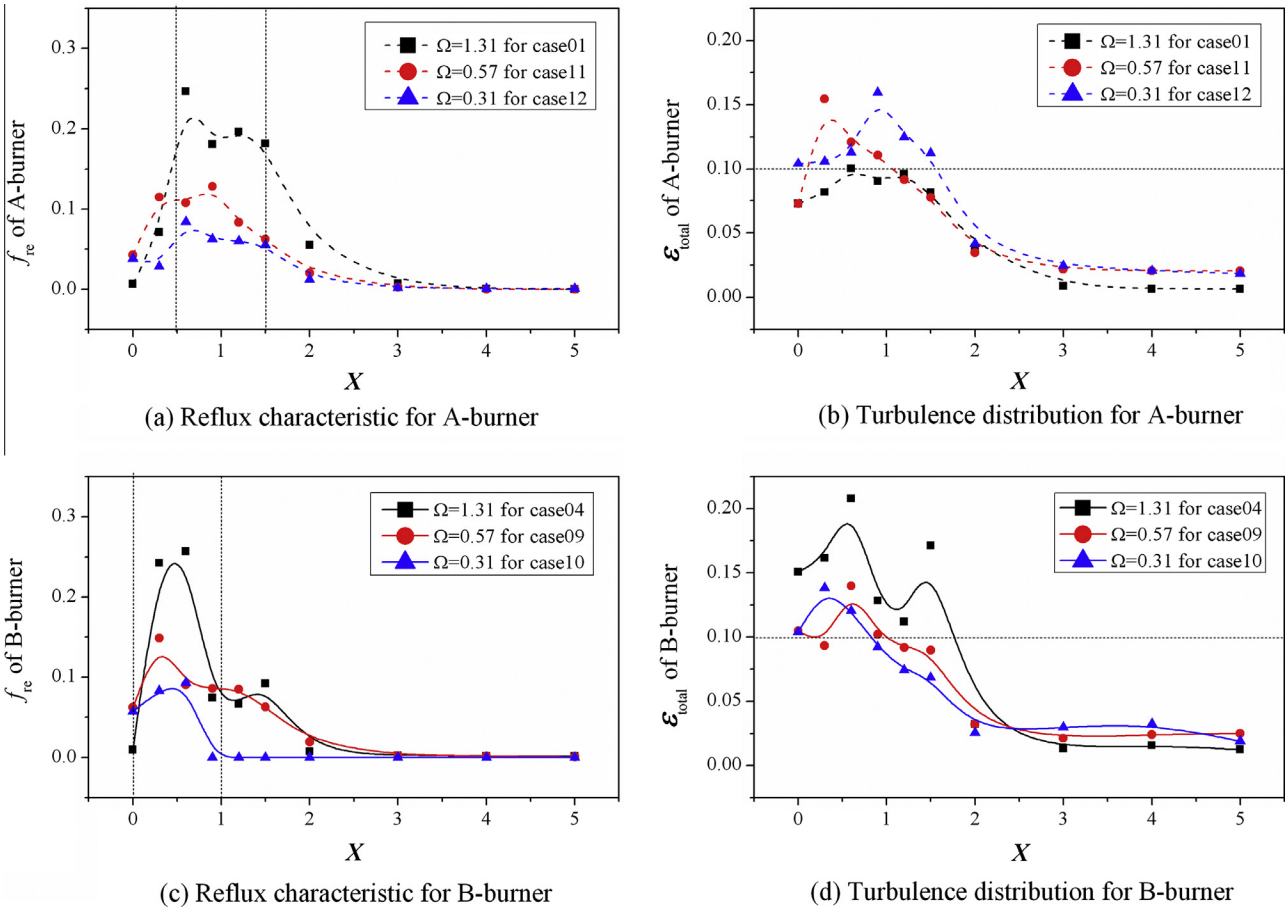

Fig. 8. Effect of swirling intensity on flow characteristic of A and B burners.

the beginning of combustion, the temperature curves down with burning bitumite and rises up with burning meager coal. The difference of temperature trend is considered as the result of volatile release characteristic. More volatile combustion for bitumite leads to the higher temperature in the beginning burning zone. In the later stage of combustion, the air flow mixing with carbon particle begins to play a dominant role in burnout period. B-burner has a less degenerative outer secondary air flow to disturb the flow field strongly as cold test results mentioned. The carbon particle will mix with oxygen more easily. Because the residence time in this pilot-scale furnace is less than that in actual boiler, coal has a limit time to be burnout. The degree of burnout will affect the later temperature level obviously. Therefore, B-burner has a better burnout for different coals, and the upper furnace has a higher temperature level with B-burner than that with A-burner.

The gas temperature of furnace outlet for the same burner is similar, so the temperature level in the upper furnace is little affected by coal type. However, the total combustion process is affected by coal type. The temperature peak of burning bitumite appears at $X = 0.4$ in the lower furnace, while the temperature peak of burning meager coal appears at $X = 0.9$ in the upper furnace. It suggests ignition of bitumite is earlier than that of meager coal because of the volatile component difference between them.

The temperature fields of cross section in lower furnace are compared between the two burners. The flow field is more stable organized by B-burner than A-burner, as mentioned in Section 3.2. Fig. 13 displays a symmetrical temperature fields in the horizontal cross-section through the burner axis and higher temperature level in the vertical cross-section for B-burner. The temperature field stability of B-burner is proved, which can be helpful to steady burning under variant working conditions. There are two temperature peaks in both two sides of the plane as shown in Fig. 13(a). Hot spot higher than 750 °C exists in the area of $X' < 0$ and $Y' < 0$, and the other hot spot area between 750 °C and 850 °C exists in the area of $Y' > 0$. In the combustion experiment both burners were under the same operation. However, because of the coal feeder instability, air supply fluctuation, and disturbance of the measurement stick through the test holes, the flow and temperature field symmetry may be disrupted a little, especially for air crash of two opposed swirl flows in a confined space. Therefore, it is important to organize a stable flow field and coal ignition in time. With the double gear rings (DGR) and dual conical flaring (DCF), the burner was proved to organize a stable flow field in cold air test. So the temperature symmetry for case IV appears to be better than that for case III. On the burner axis ($Y' = 0$), there are lower temperature gas passage for both case III and case IV. It can be explained that first air and secondary air decreased the central reverse hot flow temperature. The temperature peak appears outsides swirl flow jet off the burner spout. For both case III and IV, the temperature fields in plane $Z' = 0$ in the horizontal direction have two pieces of hot area near left and right furnace wall. The temperature difference in the two hot zones is about less than 100 °C. Moreover, the difference between number, temperature level and area of hot spots in the horizontal cross-section is also affected by the flow field fluctuation and coal combustion process organized by burner.

The vertical cross-sections for case III, IV are shown in Fig. 13(b). The most important difference in the two figures is temperature level. Under the same condition of heat load, coal type and air supply, case IV with the novel swirl burner has a higher temperature

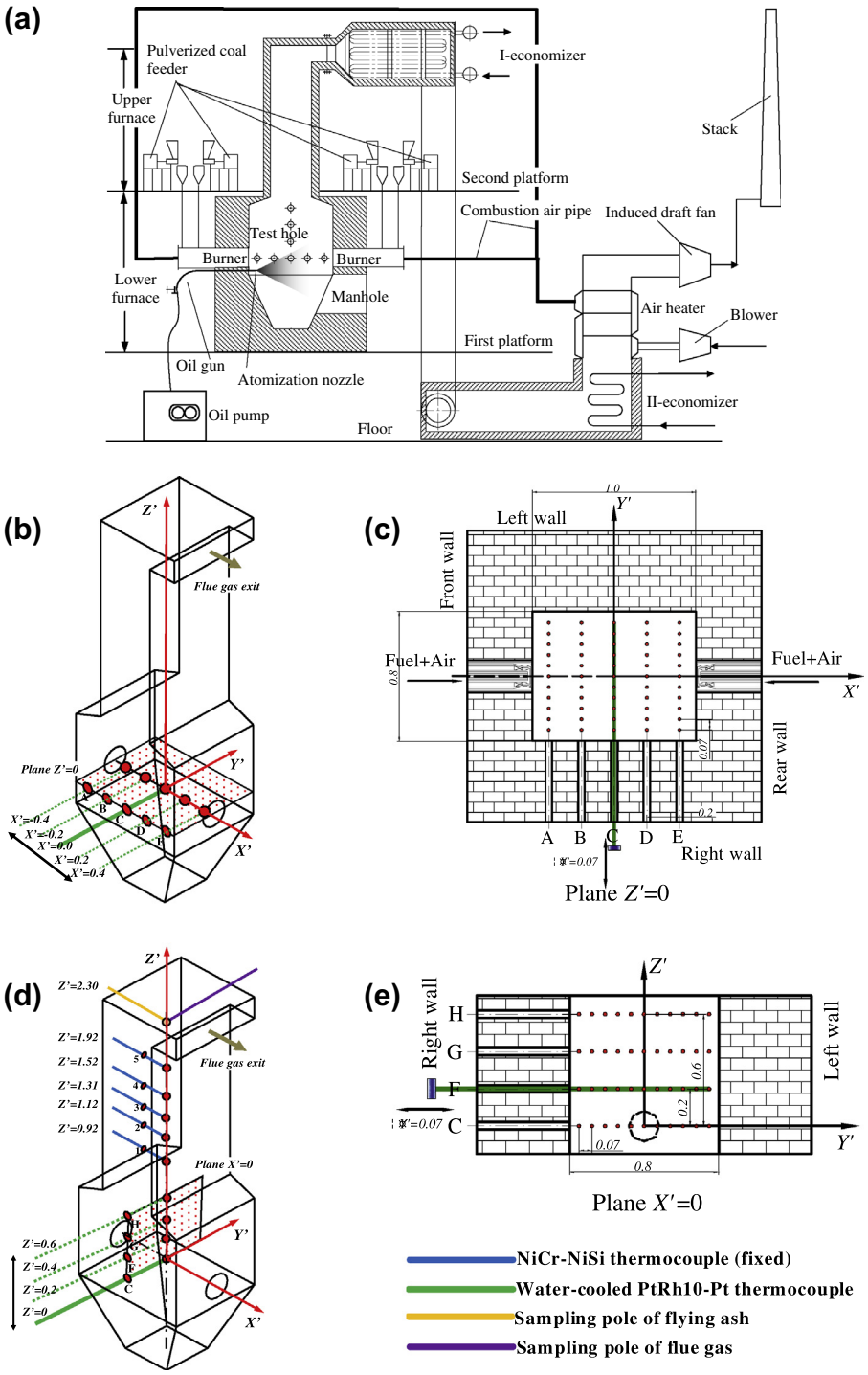

Fig. 9. Schematic diagram of combustion experimental setup (a) overall system diagram; (b) burner axis point management; (c) horizontal cross-section field point management; (d) furnace centerline point management; (e) vertical cross-section field point management.

level than case III with a traditional one. It indicates that the novel burner benefits for stable coal combustion and timely heat release. In this vertical cross-section, the zone represents the mid-term combustion just above the opposing swirl jets. The high temperature level in this zone is decided by the fresh air supply. In the cold air test, the novel burner was proved to have a stronger turbulence in the middle and later periods because of the dual conical flaring (DCF) structure. Outer secondary air can deeply penetrate the furnace center with little effect of the inner secondary air swirl jetting. Moreover, case IV has a more equable temperature level in the lower furnace along the height direction than case III, which also indicates that the pulverized coal and air mixing with novel burner is more sufficient than that with the traditional burner.

The whole Fig. 13 shows the combustion operation of burning meager coal which is difficult-flammable. The high temperature zone distributes outsides the swirl jetting off from the burner exit. Lower temperature zone exists on the burner axis which is the recirculation zone of swirling flame. High temperature gas and primary/secondary air will mix intensely in this zone so that low temperature level appears. Moreover, coal particle is less

Table 2
Coal analysis (as fired).

Name/coal type	Tongchuan (TC)	Shenmu (SM)
Proximate analysis (by weight), %		
Moisture	2.51	5.80
Ash	37.08	6.47
Volatiles	14.45	28.74
Fixed carbon	45.96	58.99
Ultimate analysis (by weight), %		
C	47.54	72.65
H	2.81	4.48
O	4.73	11.38
N	0.67	0.94
S	2.99	0.34
Q_{net}, MJ/kg	18.06	28.37
R_{90}	6.05	10.35

flammable than gas and liquid fuel, especially in the limited depth of our laboratory-scale furnace. It is possible that coal particle cannot finish combustion in the horizontal jetting section thus the flame could be lifted a little. The flame could also exist as annular shape around the swirl jetting, not located at the burner exist. The upper two plots of Fig. 13 shows high temperature zones exist on the two sides of the swirl jetting. Comparing with the vertical cross-section ($X' = 0$) temperature field, the horizontal plane ($Z' = 0$) maximal temperature is about 100 °C lower than plane $X' = 0$. It indeed illustrates that the combustion process of meager coal has not finished in the horizontal section. After opposing air flow mixing and rising, the temperature maximum forms. However, the combustion results include both two characteristic cross-section of $Z' = 0$ and $X' = 0$. The horizontal plane presents how opposed burners organize flow and temperature field in early horizontal section. For a less flammable coal, although the flame center could be lifted above this horizontal plane, the temperature level still affects the coal ignition state and combustion process in the later period. From plane $Z' = 0$, it can be seen that B-burner organized a more symmetry and higher temperature field than A-burner, which benefits for stable ignition and combustion in later period. In plane $X' = 0$ the vertical cross-section temperature level with B-burner is 130 °C more than that with A-burner. All the results mentioned above indicate the difficulty-flammable meager coal is burned more sufficiently with B-burner than with A-burner.

In this experiment, NO_x emission is also considered with being converted to $6\%O_2$. Through measuring unburned carbon percentage of fly ash C_{fh}, the char burnout can be used to evaluate the burning efficiency shown as follows [3],

$$\psi = [1 - (w_k/w_x)]/(1 - w_k) \quad (9)$$

where ψ is the char burnout, w is the ash weight fraction, and the subscripts k and x refer to the ash contents in the input coal and char sample, respectively.

Fig. 14 illustrates the compare of NO_x emission and char burnout between the two burners for two coals. The histograms for NO_x emission suggest that B-burner can help to decrease NO_x emissions with more effective burning for both coals. Because the DCF delays the mixing of primary air and secondary air, the reducing region is formed in the center. DGR concentrates pulverized coal after each gear tooth, and forms reducing region which also helps to decrease NO_x emissions. In the middle and later periods, B-burner can effectively organize the mixing of the fuel and air, and reduce the NO_x and unburned carbon in the fly ash.

4.3. Impact of secondary air distribution on B-burner

Combustion optimization has been proved to be an effective way to reduce NOx emission and unburned carbon in the fly ash [34,35]. This section mainly discusses the effect of secondary air distribution on the novel burner combustion performance with burning TC meager coal. Fig. 15 displays gas temperature on the burner axis under different air distributions. High temperature benefits ignition [33]. The temperature near burner spout rises with the increase of M, because increasing inner secondary air enhances the reverse flow effect and leaves some vortex in the wake zone near DCF. In the center of furnace, gas temperature is mainly affected by outer secondary air mixing afterwards. With M decreases, the center temperature of furnace rises because of the turbulence enhancement afterwards. However, too high gas temperature near the burner may burn down the burner spout and cause high temperature corrosion. From the whole process of pulverized coal combustion in Fig. 16, the pulverized coal ignites in the lower furnace, and burns fiercely with gas rising up. Near the throat of furnace gas temperature reaches the maximum because the cross section area of furnace becomes smaller and

Table 3
Operating conditions in combustion experiment, (Ω_1, Ω_2, $\Omega_4 = 0$, $\Omega_3 = 0.95$, $V = 0.235$ N m^3/s).

Case	Burner	Coal	Air ratio				Ω_c	M [a]
			Inner primary air (%)	Outer primary air (%)	Inner secondary air (%)	Outer secondary air (%)		
I	A	SM	15	15	50	20	0.449	1.968
II	B	SM	15	15	50	20	0.449	1.968
III	A	TC	10	10	60	20	0.566	6.378
IV	B	TC	10	10	60	20	0.566	6.378
V	B	TC	10	10	70	10	0.814	8.682
VI	B	TC	10	10	50	30	0.311	4.428

[a] Momentum ratio of inner secondary air to outer primary air.

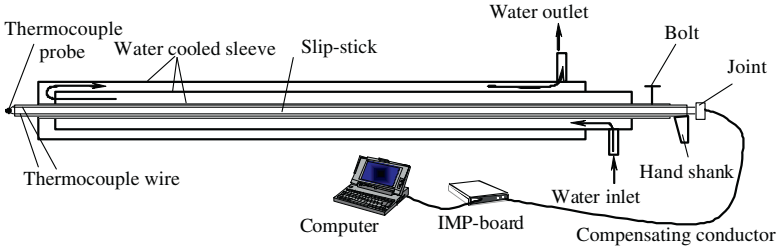

Fig. 10. Water-cooled standard PtRh10-Pt thermal couple apparatus.

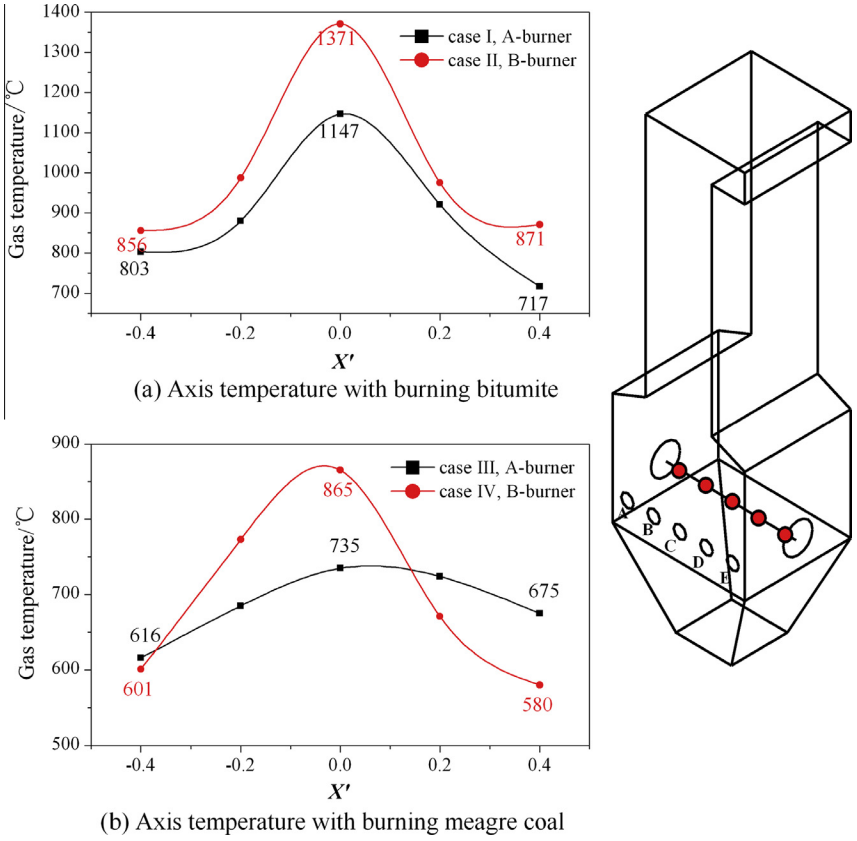

Fig. 11. Burner axis temperature comparison for different coals (case I–IV).

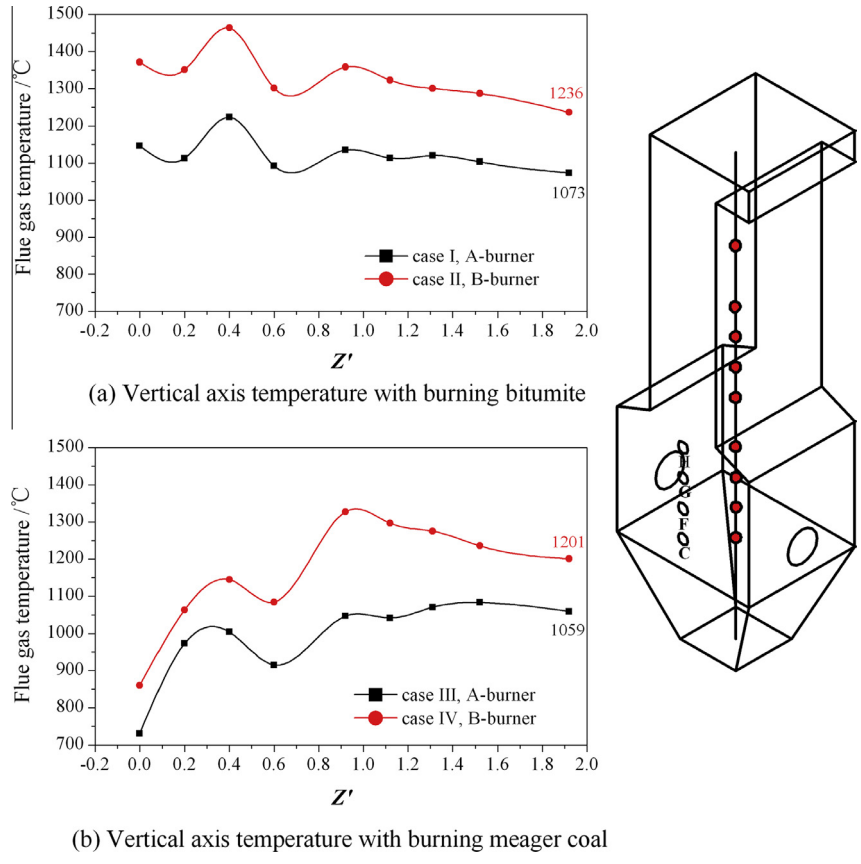

Fig. 12. Temperature change on central vertical axis for the two burners (case I–IV).

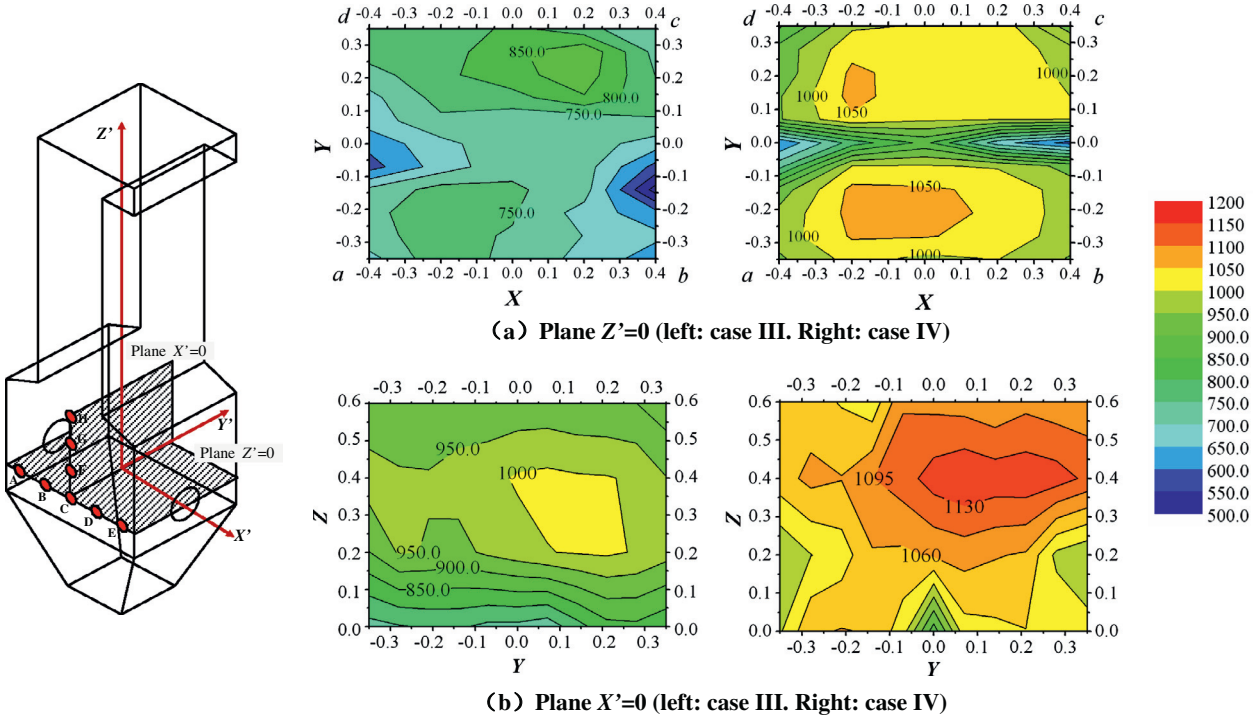

Fig. 13. Temperature field of furnace cross-section in burner zone (case III–IV) (a) temperature field in horizontal direction of cross section; (b) temperature field in vertical direction of cross section.

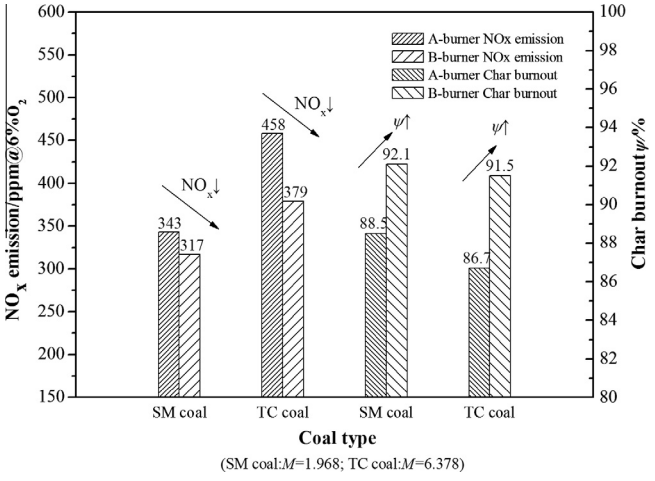

Fig. 14. NO_x emissions and char burnout compare for case I–IV.

the plan heat release rate increases. The condition of $M = 4.428$ has the highest temperature in $Z = 0$ and $Z = 1.92$, which benefits the pulverized coal ignition after leaving the spout and burnout before leaving the furnace.

To illustrate the effect of air distribution on NOx emission and combustion efficiency better, we compared NOx emission and char burnout behaviors between the two coals and different thermal loads with the novel burner in Fig. 17(a) and (b).

The effects of M on NOx emission and char burnout for the two coals are different in Fig. 17(a). For TC meager coal, the NOx emission rises up first and drops down later. The highest NOx emission exists on the condition of $M = 6.378$. The median M provides appropriate air for TC meager coal ignition and NOx formation. It is considered that lower inner secondary air ratio ($M = 4.428$) could supply the less oxygen existing in the high temperature zone and control gas temperature near the spout as Fig. 15 shows, to limit the releasing of fuel-N which hinders NOx formation. When M becomes higher ($M = 8.682$), it is inferred that DCF delays the inner

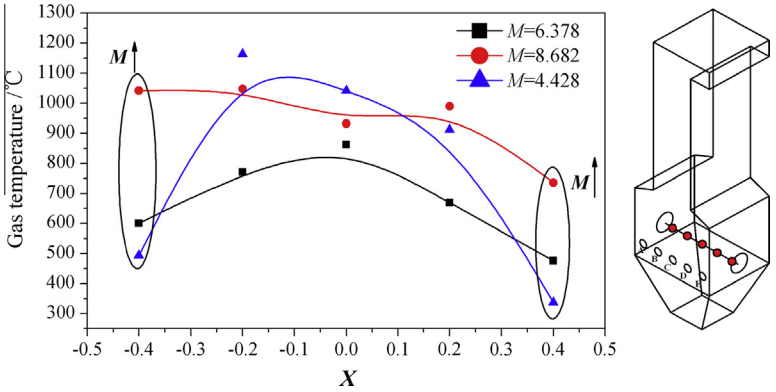

Fig. 15. Burner axis temperature distributions for case IV–VI.

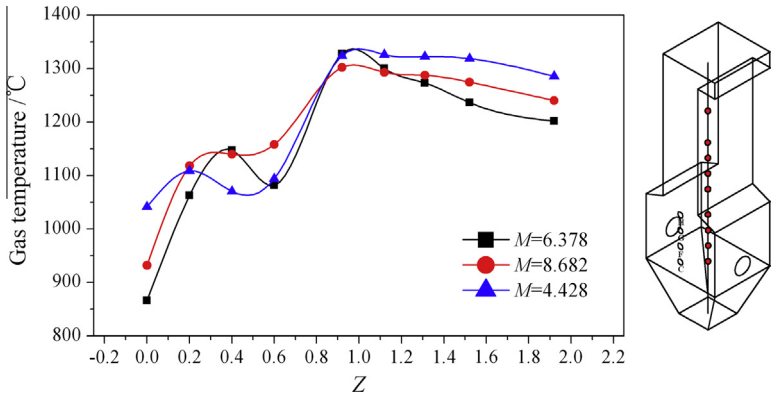

Fig. 16. Furnace center temperature of different heights for case IV–VI.

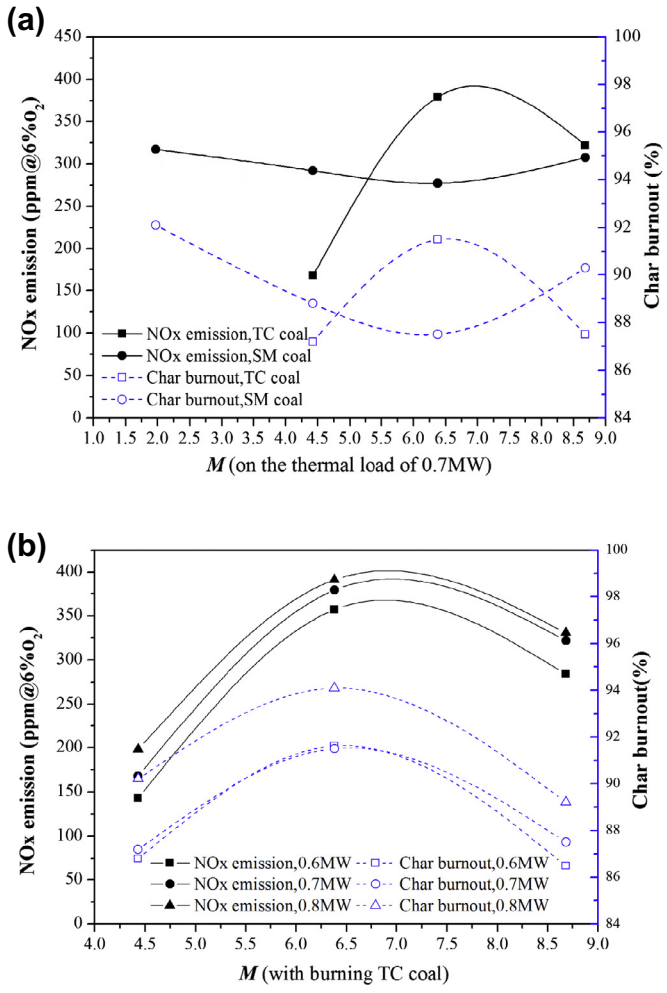

Fig. 17. NO_x emission and char burnout characteristics (a) impact of M for different two coals; (b) impact of M for different thermal loads.

secondary air and fuel mixing to reduce oxygen in the early stage, and NOx reduction could appear afterwards because of less outer secondary air supply. For SM bitumite, the NOx emission reaches the peak on the condition of $M = 1.968$ in our experiment range. Increasing M makes the NOx emission reducing. The NOx emission reaches the lowest level on condition of $M = 6.378$. It rebounds a little when the M continues to increase. The difference from the TC meager coal condition is probably caused by the volatile and oxygen content difference in the fuel. SM coal has more volatiles which induces ignition easily in the early stage. And high temperature zone exists near the air supply. Meanwhile, the oxygen content is 11.38%, more than two times of that in TC meager coal shown in Table 2, so the ignition air is sufficient. SM coal combustion generates higher NOx emission on the condition of $M = 1.968$ than TC coal NOx emission peak. However, the condition of $M = 6.378$ for SM coal could provide the appropriate air between early ignition stage and later char burnout stage which can control the NOx emission effectively. The tendency of char burnout line is similar to that of the NOx emission line for different M. It can be observed the NOx control and char burnout are contradictory. The NOx emission reducing needs to operate at the lower cost of combustion efficiency.

From Fig. 17(b) it can be observed the NOx emission changes under different thermal loads are similar with M variation. All the conditions exist the highest NOx emission level on the condition of $M = 6.378$ and lowest NOx emission level on the condition of $M = 4.428$. With the thermal load increasing, the NOx emission level rises up. The burnout lines also have the similar change rules with NOx emission lines. However, the burnout does not decrease completely with load shedding. It can be seen the char burnout of 0.8 MW is highest under different air distribution, but the difference of char burnout between 0.7 MW and 0.6 MW are not obvious. This burner is considered to have stable combustion ability under low thermal load. Comprehensively compare, the condition $M = 4.428$ is suggested in our experiment, which has a lower NOx emission for both coals and different thermal loads at a lower cost of combustion efficiency.

Although the novel burner was just studied at the experimental facility without OFA, the NOx emission obtained in our experiment can still be a valuable reference for the large scale boiler facility. The NOx formation mainly happens in the combustion zone of high temperature flame and appropriate air there. In our experiment, the combustion zone is especially studied, including flow field outside the burner spout and temperature field. The NOx emission in our study is also mainly generated in the combustion zone. Therefore, the NOx emission characteristic study of the burner is helpful to NOx control in a large facility. Moreover, the relation between NOx emission and char burnout is also discussed for the novel burner. The stable combustion efficiency could provide the convenience for NOx control. Because of the OFA installed in a large scale facility, it is believed that the air staged combustion will make the NOx emission level lower than the results in our experiment.

5. Conclusions

In this article, a novel burner spout with DGR and DCF structures based on dual register swirling burner is proposed. Cold air

test and combustion experiments are separately operated to study flow field and combustion performance of the novel burner. Reverse flow characteristic, turbulence distribution, combustion performance and NO_x emission are discussed comparing with a conventional one to verify the advantage of the novel burner in practice. The operating condition of air distribution for the novel burner is suggested.

In the cold experiment study, the novel burner has been proved to organize a great reverse flow velocity near the spout and a sufficient length of reverse flow zone. Both DGR and DCF improve the level of sectional turbulence. DGR also enhances the axial turbulence level. The novel burner has a better mass transfer performance and a more stable flow field than the conventional one.

In the combustion experiment, the novel burner can organize a more stable temperature field and better ignition condition than the conventional one. The novel burner can reduce the NO_x emission and unburned carbon in the fly ash when burning meager coal. The momentum ratio (M) of inner secondary air to outer primary air is defined to uniform the secondary air distribution. Increasing M can increase the temperature level near the novel burner spout. NO_x emissions can attain low level with $M = 4.428$ at a low cost of combustion efficiency for the two coals and under different thermal loads in the experiment range. In conclusion, the proposed burner proved to be helpful to burn pulverized coal efficiently and cleanly. The results above are valuable for the development and application of swirling burner for coal combustion.

Acknowledgment

The authors are grateful to the National Key Technology R&D Program of China (Contact No. 2011BAK06B04) and the Program for New Century Excellent Talents in University of Chinese Education Ministry (NCET-13-0458).

References

[1] H. Zhou, K.F. Cen, Experimental investigations on performance of collision-block-type fuel-rich lean burner Influence of solid concentration, Energy Fuels 21 (2007) 718–727.
[2] J. Chacón, J.M. Sala, J.M. Blanco, Investigation on the design and optimization of a low NOx–CO emission burner both experimentally and through Computational Fluid Dynamics (CFD) simulations, Energy Fuels 21 (2007) 42–58.
[3] Z.Q. Li, J.P. Jing, Z.C. Chen, F. Ren, B. Xu, H.D. Wei, Z.H. Ge, Combustion characteristics and NOx emissions of two kinds of Swirl burners in a 300-MWe wall-fired pulverized-coal utility boiler, Combust. Sci. Technol. 180 (2008) 1370–1394.
[4] S. Xue, S.E. Hui, Q.L. Zhou, T.M. Xu, Experimental study on NOx emission and unburnt carbon of a radial biased swirl burner for coal combustion, Energy Fuels 23 (2009) 3558–3564.
[5] Z.C. Chen, Z.Q. Li, Q.Y. Zhu, J.P. Jing, Gas/particle flow and combustion characteristics and NOx emissions of a new swirl coal burner, Energy 36 (2011) 709–723.
[6] J.P. Jing, Z.Q. Li, Q.Y. Zhu, Z.C. Chen, F. Ren, Influence of primary air ratio on flow and combustion characteristics and NOx emissions of a new swirl coal burner, Energy 36 (2011) 1206–1213.
[7] Y.G. Zhou, M.C. Zhang, T.M. Xu, S.E. Hui, Effect of opposing tangential primary air jets on the flue gas velocity deviation for large-scale tangentially fired boilers, Energy Fuels 23 (2009) 5375–5382.
[8] X.L. Wei, Y. Wang, D.F. Liu, H.Z. Sheng, W.D. Tian, Y.H. Xiao, Release of sulfur and chlorine during cofiring RDF and coal in an internally circulating fluidized bed, Energy Fuels 23 (2009) 1390–1397.
[9] H. Xu, S.T. Zhang, X.B. Lu, Y. Liu, X.Y. Yu, Effect of ultrasound on SO_2 desorption from sodium alkali desulphurization regeneration solution, Chem. Eng. Technol. 33 (2010) 231–236.
[10] Y. Li, H.Y. Qi, J. Wang, SO_2 capture and attrition characteristics of a CaO/bio-based sorbent, Fuel 93 (2012) 258–263.
[11] Z.Y. Wen, C. Zhang, Q.Y. Fang, G. Chen, Feasibility Study on accessorial limestone injection desulfurization system on large capacity boiler, in: J.Y. Yan, C.C. Zhou, R. Liao, J.W. Wang (Eds.), Electrical Power & Energy Systems, Pts 1 and 2, Trans Tech Publications Ltd., Stafa-Zurich, 2012, pp. 293–301.
[12] X.L. Wei, Y. Wang, D.F. Liu, H.Z. Sheng, Influence of HCl on CO and NO emissions in combustion, Fuel 88 (2009) 1998–2003.
[13] S.S. Daood, M.T. Javed, B.M. Gibbs, W. Nimmo, NOx control in coal combustion by combining biomass co-firing, oxygen enrichment and SNCR, Fuel 105 (2013) 283–292.
[14] J.P. Smart, G.J. Nathan, N.L. Smith, G.J.R. Newbold, D.S. Nobes, D.J. Morgan, On the development of a coal fired precessing jet burner, IFRF Combust. J. 02 (1999) 1–21.
[15] M. Costa, J.L.T. Azevedo, M.G. Carvalho, Combustion characteristics of a front-wall-fired pulverized-coal 300 MWe utility boiler, Combus. Sci. Technol. 129 (1997) 277–293.
[16] U. Bollettini, F.N. Breussin, R. Weber, A study on scaling of natural gas burners, IFRF Combust. J. 06 (2000) 1–24.
[17] A. Milani, A. Saponaro, Diluted combustion technologies, IFRF Combust. J. 01 (2001) 1–32.
[18] M.A. Nettleton, The influence of swirl angles on flame stability in pilot-scale plant, Fuel 83 (2004) 253–256.
[19] M. Gu, M. Zhang, W. Fan, L. Wang, F. Tian, The effect of the mixing characters of primary and secondary air on NO formation in a swirling pulverized coal flame, Fuel 84 (2005) 2093–2101.
[20] J.P. Jing, Z.Q. Li, G.K. Liu, Z.C. Chen, F. Ren, Influence of different outer secondary air vane angles on flow and combustion characteristics and NOx emissions of a new Swirl coal burner, Energy Fuels 24 (2010) 346–354.
[21] Z.Q. Li, J.P. Jing, G.K. Liu, Z.C. Chen, C.L. Liu, Measurement of gas species, temperatures, char burnout, and wall heat fluxes in a 200-MWe lignite-fired boiler at different loads, Appl. Energy 87 (2010) 1217–1230.
[22] A.D. LaRue, J.J. Wolf, Mixer for Dual Register Burner, United States Patent, No.4,380,202, 1983.
[23] S. Morita, T. Masai, S. Nakashita, T. Uemura, F. Kouda, T. Nawata, Apparatus for Coal Combustion, United States Patent, No.4,545,307, 1985.
[24] J. Vidal, F. Malaubier, J.C. Mevel, Ignition and Combustion Supporting Burner for Pulverized Solid Fossil Fuel and Combustion Chamber Comprising Same, United States Patent, No.4,690,075, 1987.
[25] A.D. LaRue, Burner for Coal, Oil or Gas Firing, United States Patent, No.4,836,772, 1989.
[26] M. Fantui, L. Ballarino, Industrial applications of Tenova FlexyTec (R) flameless low NOx burners, Rev. Metall. 105 (2008) 194–205.
[27] N.G. Orfanoudakis, A. Hatziapostolou, K. Krallis, E. Mastorakos, K. Sardi, D.G. Pavlou, N. Vlachakis, Design, evaluation measurements and modelling of a small swirl stabilised laboratory burner, IFRF Combust. J. 10 (2005) 1–29.
[28] C. Allouis, R. Pagliara, A. Saponaro, Fast infrared imaging for combustion stability analysis of industrial burners, Exp. Therm. Fluid Sci. 43 (2012) 2–8.
[29] K. Khanafer, S.M. Aithal, Fluid-dynamic and NOx computation in swirl burners, Int. J. Heat Mass Transfer 54 (2011) 5030–5038.
[30] G.G. Sun, D.F. Che, Z.H. Chi, Effects of secondary air on flow, combustion, and NOx emission from a novel pulverized coal burner for industrial boilers, Energy Fuels 26 (2012) 6640–6650.
[31] Z.G. Li, Similarity and modeling: Theory and Application, National Defence Industry Press, Beijing, 1982.
[32] A.S. Veríssimo, A.M.A. Rocha, M. Costa, Importance of the inlet air velocity on the establishment of flameless combustion in a laboratory combustor, Exp. Therm. Fluid Sci. 44 (2013) 75–81.
[33] Q. Zhou, Q. Zhao, N. Li, X. Chen, T. Xu, S. Hui, A dimensionless factor characterizing the ignition of pulverized coal flow: analytical model, experimental verification, and application, Int. J. Energy Res. 33 (2009) 235–254.
[34] S. Zhao, S.E. Hui, L. Liang, Q.L. Zhou, Q.X. Zhao, N. Li, H.Z. Tan, T.M. Xu, Effect of the momentum flux ratio of vertical to horizontal component on coal combustion in an arch-fired furnace with upper furnace over-fire air, Exp. Therm. Fluid Sci. 45 (2013) 180–186.
[35] F. Wu, H. Zhou, J.P. Zhao, K.F. Cen, A comparative study of the multi-objective optimization algorithms for coal-fired boilers, Expert. Syst. Appl. 38 (2011) 7179–7185.